Materials Advances

ROYAL SOCIETY OF CHEMISTRY

PAPER

View Article Online
View Journal | View Issue

Cite this: *Mater. Adv.*, 2025, 6, 6427

Biodegradable polyhydroxyalkanoate (PHA) composites with biochar ratios optimized for the additive manufacturing method of material extrusion: engineering, rheological, and morphological insights†

Nectarios Vidakis,[a] Nikolaos Michailidis,[bc] Dimitrios Kalderis,[d] Apostolos Argyros,[bc] Katerina Gkagkanatsiou,[a] Maria Spyridaki,[a] Ioannis Valsamos,[a] Vassilis Papadakis[ef] and Markos Petousis *[a]

Naturally derived poly(hydroxyalkanoate) (PHA) and biochar from agricultural residues were combined to develop an environmentally friendly, completely biodegradable composite with improved thermal and mechanical properties. Six filler concentrations (0.0, 0.5, 1.0, 1.5, 2.0, and 2.5 wt%) were prepared to extrude into filaments and subsequently manufacture the respective 3D printed composites through material extrusion (MEX) additive manufacturing (AM). The samples discussed here are bio-originated composites, and as a consequence, they can potentially be a revolutionary replacement for environmentally harmful, industrially produced polymeric materials, at the appropriate and desired applications. 3D printed PHA/biochar composites have potential for use across a range of industrial applications such as packaging, agriculture, prototyping, and environmental monitoring, where sustainability and biodegradability are requirements. Still, their industrialization involves several challenges, such as the brittleness of PHA, the interaction with the biochar, and possible printability issues that need to be addressed. The samples were subjected to several tests to assess their rheological, thermal, and mechanical properties, as well as their structure and morphology. Thermogravimetric analysis, dynamic mechanical analysis, differential scanning calorimetry, tensile tests, bending tests, microhardness, and Charpy impact tests were conducted. In addition, the porosity and dimensional accuracy were evaluated, while scanning electron microscopy and, by extension, energy dispersive spectroscopy were used to assess microstructure formation. The obtained results indicated enhanced performance in the biochar 0.5 wt% compound in terms of tensile (17.7% increase) and bending toughness (3.1% increase), bending strength (32.8 MPa, 15.3% increase), and Charpy (1.9% increase) impact strength, and for PHA/1.0 wt% biochar composites regarding tensile strength (22.1 MPa, 15.3% increase), Young's modulus (131.5 MPa, 25.4% increase), dimensional accuracy (better by 11.2%), and porosity (reduced by 23.3%).

Received 23rd March 2025,
Accepted 24th July 2025

DOI: 10.1039/d5ma00266d

rsc.li/materials-advances

1. Introduction

Numerous environmental concerns originate from the overuse of plastics and other materials derived from natural resources, which contribute to climate change, pollution, and fossil fuel depletion.[1] The adoption of eco-friendly biopolymers offers a promising solution for plastic-related pollution owing to their biodegradability and biocompatibility.[2–4] Given the growing global emphasis on sustainable development, these materials have received significant attention.[5]

Efforts have been made to manage waste by developing methods for reuse and repurposing, with the aim of minimizing the environmental footprint. With appropriate treatment

[a] Department of Mechanical Engineering, Hellenic Mediterranean University, Heraklion 71410, Greece. E-mail: markospetousis@hmu.gr; Tel: +302810379227
[b] Physical Metallurgy Laboratory, Mechanical Engineering Department, School of Engineering, Aristotle University of Thessaloniki, 54124 Thessaloniki, Greece
[c] Centre for Research & Development of Advanced Materials (CERDAM), Center for Interdisciplinary Research and Innovation, Balkan Centre, Building B', 10th km Thessaloniki-Thermi road, 57001, Thessaloniki, Greece
[d] Department of Electronic Engineering, Hellenic Mediterranean University, Chania 73133, Greece
[e] Department of Industrial Design and Production Engineering, University of West Attica, 122 43 Athens, Greece
[f] Institute of Electronic Structure and Laser, Foundation for Research and Technology–Hellas, N. Plastira 100m, 70013 Heraklion, Greece

† Electronic supplementary information (ESI) available. See DOI: https://doi.org/10.1039/d5ma00266d

and processing, various types of waste can be transformed into valuable materials for bio-based product manufacturing, bioenergy production, and other applications, fostering a circular bioeconomy.[6] Three-dimensional printing (3D-P) plays a significant role in this bio-based transition by employing bio-based materials for manufacturing across various sectors.[7] The global market for bio-based manufacturing processes involves the production of chemicals, materials, and products derived from renewable biological feedstock such as biomass. According to a survey from Spherical Insights (2025),[8] the global bio-based chemicals market was valued at approximately USD 73.10 billion in 2023 and is expected to surpass USD 177 billion by 2030, growing at a compound annual growth rate (CAGR) of around 9.25%. The bio-based polymer market is expected to exceed USD 30 billion by 2027, driven by the increased demand in packaging, automotive, and consumer goods industries.[9]

The core principle of 3D printing technology[10–12] is the deposition of materials in a layer-by-layer fashion.[13] This cost-effective manufacturing method facilitated the fabrication of complex designs.[14–16] This process relies on digital model data.[17] Compared to conventional methods, 3D printing offers several advantages,[13] including reduced production costs (for small production batches, as the cost of AM produced products is the same, irrespective of the amount of the produced products, while for products based on conventional methods, the cost is reduced as the number of produced products increase), improved time efficiency, and the ability to fabricate intricate geometries.[18,19] It is widely applied in various industries such as aerospace,[20] automotive,[21] food,[22] medical,[23] healthcare,[24] architecture, construction,[25] and electronics.[26,27]

A wide range of materials can be utilized, including polymers,[28,29] ceramics,[30] metals,[31] composites,[32,33] and smart or specialized materials.[26] Commonly used and studied polymers in the material extrusion (MEX) method in Additive Manufacturing include polypropylene (PP),[34] acrylonitrile butadiene styrene (ABS),[35] polylactic acid (PLA),[36] polyamides,[37] or even polyethylene terephthalate glycol (PETG).[38] Biopolymers and their composites are widely used in various applications and are expected to gain more prominence in the future,[39] with the aim of replacing petroleum-based polymers.[40,41] Common biopolymers used in 3D printing include polycaprolactone (PCL),[42–44] polylactic acid (PLA),[45–47] polyhydroxybutyrate (PHB),[48] poly(butylene succinate) (PBS),[49] and poly(hydroxy alkanoates) (PHAs).[50]

Polyhydroxyalkanoates are biodegradable polymers that are synthesized by a diverse range of bacteria in the form of intracellular granules.[51] Numerous bacterial and archaeal species can be used for the natural synthesis of PHAs.[52–54] Based on their mechanical properties, PHAs can be classified as short-chain-length polyhydroxyalkanoates (PHASCL) or medium-chain-length polyhydroxyalkanoates (PHAMCLs). First, the monomer unit contains no more than five carbon atoms, whereas in the second, it contains more than five atoms.[55] PHAs are promising natural alternatives[56] to petrochemical-based polymers.[57]

PHA can be employed as a bio-based additive to develop composites when combined with materials such as PLA.[58,59] Its use is increasing.[60] PHA was combined with PLA, and its thermophysical and rheological properties were investigated under various processing conditions and filler additions.[61] The results indicated that the composites' processability was enhanced, with the nozzle temperature identified as the most influential parameter affecting the mechanical characteristics.

Several reports have analyzed and predicted the global PHA market size, providing detailed information, including compound annual growth rate (CAGR) values. In the forecast period of 2024–2031, the market size is expected to rise from $105.42 million to $160.56 million, reflecting a 5.40% CAGR.[62] Similarly, for the 2022–2029 forecast period, the global PHA market value is expected to increase from USD 73.12 million to USD 128.0 million.[63] In another report,[64] it is forecasted that throughout 2024–2034, the market will experience an 8.9% CAGR, with the market size rising from USD 123.5 million in 2024 to USD 298.3 million in 2034.

Bioproducts can be created when biomass undergoes pyrolysis, gasification, or hydrothermal carbonization. Pyrolysis is commonly employed for the conversion of biomass into value-added products, specifically syngas, bio-oil, and biochar.[65] Proper valorization of products such as biochar can have a positive impact on economic viability and promote environmental sustainability,[65] provided that production is cost-effective[66] and not competitive with existing biomass valorization practices.[67,68]

Carbon-based additives are commonly used as fillers in composites in 3D printing.[69,70] Biochar is a carbon-based material, which is defined as a solid material produced by thermochemically converting biomass under oxygen-limited conditions.[71] Biochar properties may vary depending on the type of biomass and the treatment temperature.[72,73] Several types of biochar can be derived from various feedstocks[74] including wood residues,[75] animal manures,[76] sewage sludge,[77] crop straw,[78] food wastes,[79] and others.[80,81] The biochar source material and production process affect its properties. Thus, there are numerous studies on biochar, sourced from different natural waste.[10,11,82–84]

It exhibits high porosity, stability, a large surface area, and other beneficial properties that are useful for various applications.[85] Some of the most common applications of biochar include soil remediation,[86–88] water treatment,[89–91] carbon capture or air filtration,[92–94] heat and power production, flue gas cleaning,[95] metallurgical processes,[96] agricultural applications,[97] building materials[98] and medical applications.[99] The advantages of biochar, such as its eco-friendliness, reusability, and cost-effectiveness,[100,101] are among the reasons for its increasing utilization not only by the research community but also by the manufacturers.

These findings are supported by various reports on the biochar market size and projections, as well as by existing literature. It is estimated that between 2024 and 2031, the market revenue will rise from $231.4 million in 2023 to $700.7 million by 2031, reflecting a 13.1% CAGR. According to another report,[102] the global market of biochar was estimated at $680.84 million in 2023 and is expected to increase from $763.48 million in 2024 to $2097.0 million by 2032, with a 13.47% CAGR. Additionally, projections show[103] that

the biochar market, valued at USD 253.29 in 2023, will grow at approximately 14.0% between 2024 and 2030, reaching about USD 622.8 million by 2030.

Various studies have investigated the utilization of biochar to enhance the response of polymeric materials in different applications. For example, the mechanical performance of PLA/biochar (BC) composites after 3D printing was parametrically studied,[104] which demonstrated enhancements in the tensile strength and bending stiffness.

Biochar was incorporated as filler (0–1 wt%) into a polypropylene (PP) matrix.[105] The produced samples were examined for surface morphology and mechanical and thermal characteristics. The findings revealed an improvement in tensile strength and improved thermal stability. In a separate study, PET/biochar composites were fabricated and tested, and the outcome indicated that the introduction of biochar enhanced the mechanical, thermal, and dynamic properties of the compounds.[106] Furthermore, this group has previously demonstrated the benefits of combining biochar samples with conventional, non-degradable polymers, in material extrusion (MEX) 3D printing, such as polylactic acid (PLA),[107] polypropylene (PP),[108] acrylonitrile butadiene styrene (ABS),[109] and high-density polyethylene (HDPE).[110] The findings show a strong potential for the use of biochar as an eco-friendly reinforcing agent (filler) for conventional 3D printing polymers. For instance, for the PP thermoplastic,[108] the tensile strength was improved by 28.4% with 4 wt% biochar content in the composites. The effect of biochar as a filler on the quality characteristics of such polymers has also been reported,[111] while the overall effect of 3D printing polymeric materials has been summarized in literature studies.[112]

In this research, PHA/biochar composites were fabricated with six different filler concentrations (0.0, 0.5, 1.0, 1.5, 2.0, and 2.5 wt%). Combining PHA with biochar has the added advantage of developing 100% biodegradable composites, thus promoting circular bio-economy and environmental protection. The investigation carried out into the literature did not reveal any similar study so far. Initially, mixtures were formed with raw materials, which were subsequently extruded into filaments suitable for 3D printing. The printed specimens were then formed into the desired shape prior to testing and evaluation in accordance with the relevant standards. The tests included assessments of both filaments and specimens for thermal and rheological behavior, as well as mechanical and morphological characteristics. The thermal behavior was evaluated by measurements implemented with the thermogravimetric analysis (TGA) method and the differential scanning calorimetry (DSC) method. Rheological properties were investigated using viscosity measurements. The material flow rate (MFR) analysis was also implemented. The mechanical properties were assessed by testing the tensile and bending responses of the manufactured samples, as well as their Charpy impact and microhardness. Furthermore, thermomechanical dynamic mechanical analysis (DMA) was also carried out. Additionally, the morphologies of the samples and biochar were assessed by energy dispersive spectroscopy (EDS) and scanning electron microscopy (SEM). The geometrical accuracy and the voids of the samples were examined with the sophisticated and accurate micro-computed tomography (μ-CT) method. These two aforementioned metrics are related to the quality characteristics of the 3D printing structure. The experimental findings showed that it is possible to produce 100% biodegradable composites for the MEX AM method. The capability of biochar to enhance the mechanical behavior of polymeric matrices was once again verified in this biosynthesized PHA biopolymer, showing strong potential for applying 100% eco-friendly composites in the MEX AM method.

2. Materials and methods

The experimental workflow of this work is illustrated in Fig. 1, detailing the procedures from raw materials through filament and specimen fabrication to the evaluation of the mechanical, thermal, rheological, morphological, and structural properties. Fig. 1(a) and (b) depict the weighing and drying of PHA and biochar raw materials. Fig. 1(c)–(e) show the filament melt extrusion, subsequent drying, and preliminary mechanical testing, respectively, while Fig. 1(f) illustrates the fabrication of the parts (MEX AM). Fig. 1(g)–(i) show the experimental process for the mechanical testing of the printed examples, and Fig. 1(j)–(l) display the rheological, thermal, and morphological characterization of the parts.

2.1. Materials

PHA and biochar materials were used for this investigation. PHA was supplied by ColorFabb (Belfeld, the Netherlands) under the trade name AllPHA ColorFabb pellets. According to the technical datasheet provided by the supplier, this material is produced by fermentation (a natural process), where bacteria convert natural sugars and oils into PHA by accumulating intracellular lipid granules. Biochar was produced by this research team from pruning olive trees collected in Chania, Crete, Greece. The biomass was first washed to remove impurities and then air dried. Flame curtain pyrolysis was used as the fabrication method, and more details and specifications can be found here.[113] The rest of the steps are described in detail in ref. 107. The produced samples were thoroughly ground using a Sepor-type rod mill. Fig. 2(a) shows the SEM picture of the biochar particles captured at a magnification of 1600×, while Fig. 2(b) and (c) show SEM images taken at 70 000× and 130 000× magnifications, respectively.

2.2. Materials formulation, production of the filament, and the specimens

The two raw materials were processed employing a high-power blender for 20 minutes (operating at 4000 rpm). Six different blends of biochar and PHA were prepared: 0.0, 0.5, 1.0, 1.5, 2.0, and 2.5 wt% of biochar particle loading. The range of filler quantities was selected based on preliminary tests conducted, up to the point where a further increase in the biochar content no longer enhanced the mechanical properties in the

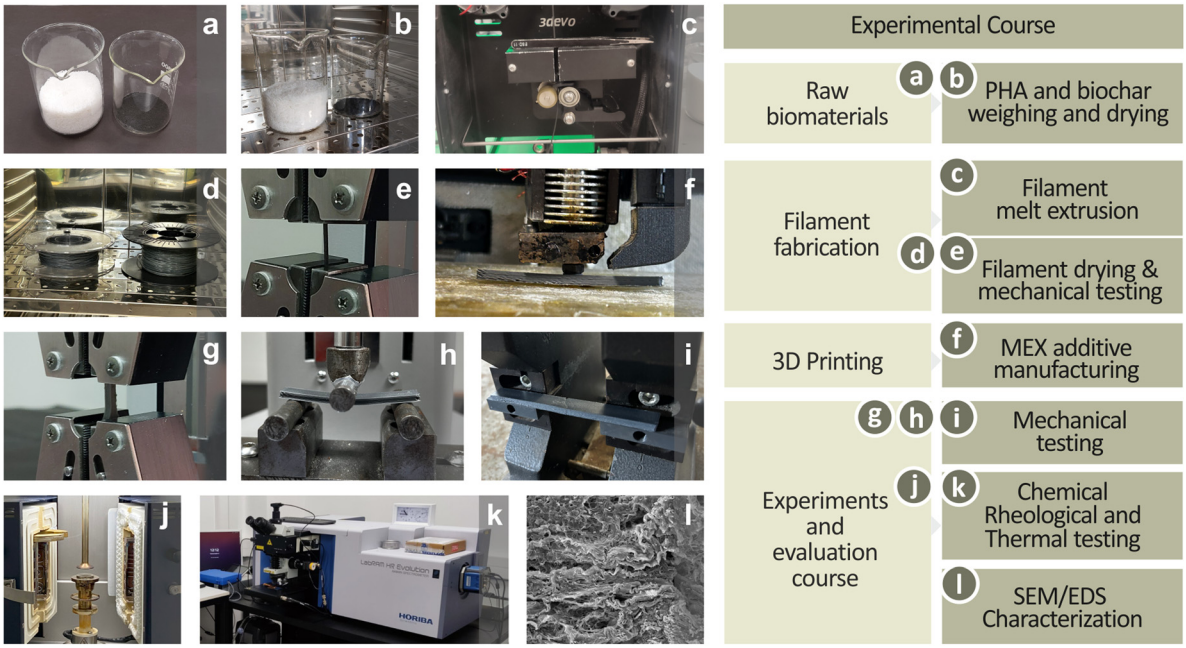

Fig. 1 (a) and (b) PHA and biochar weighing and drying, (c)–(e) filament extrusion, drying, and mechanical testing, (f) specimen fabrication through MEX AM, (g)–(i) mechanical testing of specimens, (j) and (k) rheological and thermal characterization, and (l) morphological analyses by SEM and EDS.

composites (saturation phenomena[114,115]). The produced filament was 1.75 mm in diameter to meet the requirements of the 3D printer machine. This extruder is specially designed for material mixing and the production of filaments specifically for the MEX AM method. This is a commercially available extruder from the 3devo company (Composer 450, Utrecht, the Netherlands). It features a screw developed with geometric characteristics aiming to facilitate the materials mixing process, therefore achieving good dispersion of the additives, as the manufacturer claims. This was afterward verified by SEM and EDS of the samples, along with analysis of the experimental results.

For the fabrication of the 3D samples, a MEX AM Intamsys Funmat HT (INTAMSYS Technology Co. Ltd, Shanghai, China) was used. Four types of specimens were manufactured to perform tensile, bending, Charpy, and dynamic mechanical analyses (DMA) experiments. The printing parameters and their dimensions are illustrated in the ESI.† The specimens were printed with a 0.4 mm nozzle. The nozzle temperature was 200 °C, the build plate was 40°, a ±45° rectilinear infill pattern was used, and an orientation angle of 0°. Each specimen was printed with 2 perimeters, no solid layers on the top or bottom, a 0.2 mm layer height, and a printing speed of 50 mm s^{-1}.

Samples with various types of typical prismatic and curvature geometric features were also prepared by the authors to evaluate the 3D printed samples' geometric accuracy with the μ-CT scanner apparatus. The same was used for the evaluation of the pores formed during the building of the examples in the 3D printing structure.

2.3. Raman characterization, rheology, and thermal examination

Raman peaks were assessed with a LabRAM HR Raman Spectrometer from HORIBA Scientific, located in Kyoto, Japan. For the rheology property assessment, a DHR-20 Discovery Hybrid Rotational Rheometer from TA Instruments, located in New Castle, Delaware, in the United States, was used. Regarding the melt flow rate (MFR) tests, the temperature used was the one

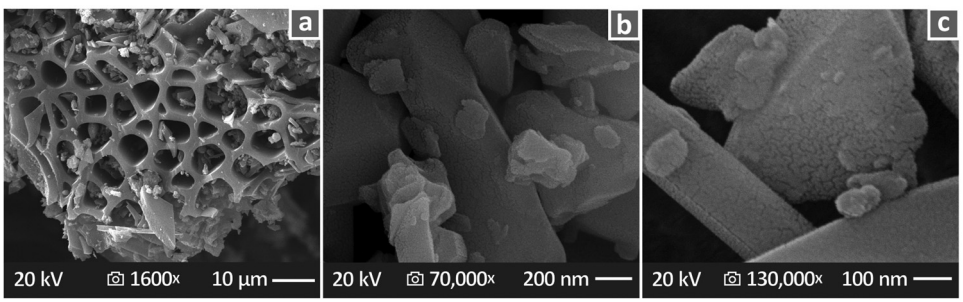

Fig. 2 SEM images of biochar at (a) 1600×, (b) 70 000, and (c) 130 000× magnifications.

provided by the ASTM D1238. Regarding the viscosity measurements, the temperature applied was selected to be close to the nozzle temperature during the 3D printing process. Moreover, a model named Diamond (TGA, PerkinElmer, Waltham, U.S.) and a DSC 25 (DSC, TA Instruments, New Castle, U.S.) were used for the assessment of the effect of biochar on the thermal response of PHA. The methodology can be found in the ESI.†

2.4. Mechanical testing

Mechanical experiments were carried out on the fabricated PHA/biochar specimens for each filler concentration. Tensile and bending experiments were performed employing an MX2 motorized test stand from Imada Inc., located in Tokyo, Japan. The instrument featured the appropriate grips. ASTM D638-14 (type V, 3.2 mm thickness) and ASTM D790-10 (52 mm clearance in the supports) standards were used, and tests were implemented with 10 mm min^{-1} elongation speed. For the impact test (Charpy notched), an MT220 device from Terco AB, located in Kungens, Sweden, was employed following the instructions of the ASTM D6110 standard (367 mm hammer release height). With regard to the Vickers microhardness tests, a Test 300-Vickers instrument from Innovatest Europe BV, established in Maastricht, the Netherlands, was used. Measurements were carried out in accordance with the ASTM E384-17 standard. All experiments were carried out under ambient conditions.

Additionally, DMA was conducted using a Discovery Hybrid Rheometer DHR20 equipped with a 3-point bending setup and a 40 mm span. The examination covered a temperature range from 30 to 190 °C, with the temperature increasing at a rate of 5 °C min^{-1}. Throughout the analysis, the sample was subjected to sinusoidal strains between 0 and 0.05% at a frequency of 1 Hz. To maintain consistent contact with the specimen during the entire testing process, a force-tracking mechanism was employed.

2.5. Micro-computed tomography, SEM, and EDS

The structures of the fabricated examples were inspected with micro-CT with a Tomoscope HV Compact instrument (Werth-Messtechnik GmbH, Germany). The geometrical deviation and voids of the MEX 3D-fabricated specimens were analyzed, and the resulting data were correlated with the mechanical test outcomes. SEM inspection was conducted on both the biochar particles and the fabricated PHA/biochar specimens, using an SEM field emission device model named JSM-IT700HR from JEOL Ltd, located in Tokyo, Japan. Pictures were acquired from the lateral and fractured sections of the samples at different magnifications to thoroughly assess their morphology and correlate the findings with those derived from mechanical tests. EDS allowed the elemental assessment of the samples examined.

3. Results

3.1. Raman evaluation

Fig. 3 depicts the Raman spectral profiles for unfilled PHA and the PHA/biochar mixtures (Fig. 3(a)) as well as the resulting spectra after subtracting the unfilled PHA from those of the PHA/biochar compounds at filler concentrations of 0.0, 0.5, 1.0, 1.5, 2.0, and 2.5 wt% (Fig. 3(b)). Table 1 presents the Raman peaks for the unfilled PHA documented with the respective literature.

As illustrated in Fig. 3(b), the addition of biochar to PHA has induced several changes in Raman intensity. In particular, in the three Raman peaks (60, 447, and 611 cm^{-1}), the intensity exhibited a small decrease, while at 81, 841, 1727, 2930, 2974, and 3000 cm^{-1}, the intensity increased. The Raman peaks at 2930, 2974, and

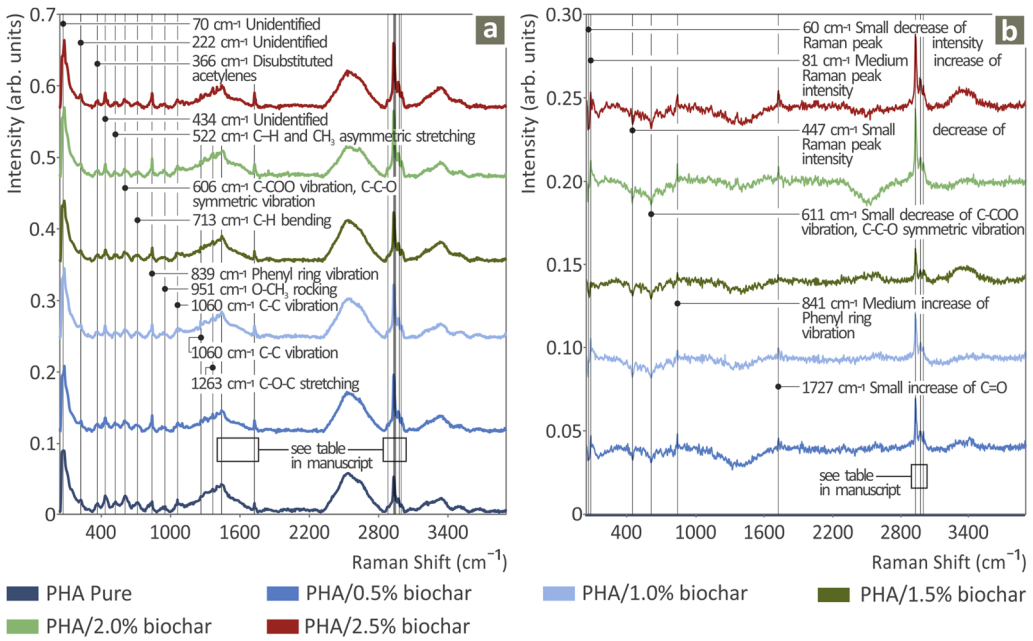

Fig. 3 Raman derived data for pure PHA and PHA/biochar (0.5, 1.0, 1.5, 2.0, and 2.5 wt%) composite samples, in intensity *vs.* Raman shift graphs: (a) Raman spectra and (b) the result after subtracting the unfilled PHA from all PHA/biochar compounds (please see Table 1, as well).

Table 1 Major Raman peaks for the unfilled PHA accompanied by the related assignments

Wavenumber (cm^{-1})	Intensity	Raman peak assignment
70	Strong	Unidentified
222	Small	Unidentified
366	Small	Disubstituted acetylenes[116]
434	Medium	Unidentified
522	Small	C–H and CH_3 asymmetric stretching[117]
606	Medium	C–COO vibration, C–C–O symmetric vibration[117]
713	Small	C–H bending[118]
839	Medium	Phenyl ring vibration[118,119]
951	Small	O–CH_3 rocking[117]
1060	Medium	C–C vibration[120]
1263	Small	C–O–C stretching[117]
1364	Medium	C–C–H, C–O–H, and O–C–H[121]
1440	Medium	CH_3 asymmetric stretching[122]
1725	Medium	C═O bond stretching;[117,123] C–O–C symmetric stretching[124]
2880	Small	CH_2, CH_3 vibration[120]
2930	Very strong	CH_2 asymmetric stretching; CH vibration[116]
2938	Small	CH_2 asymmetric stretching[121]
2947	Small	CH_2 asymmetric stretching[121]
2979	Strong	C–H stretching[119]
2996	Medium	C–H stretching[119]

3000 cm^{-1} experienced strong, moderate, and slight gradual increases, respectively. Notably, the expected graphite bands, the D-band at 1340 cm^{-1} and the G-band at 1590 cm^{-1}, which are commonly found in biochar, were not found in the measurements, probably because of the high photoluminescence of the samples. All changes presented with the related assignments are shown in Table 2.

3.2. Rheological and thermal characterization

Fig. 4 presents the rheological characteristics of the PHA/biochar composites at filler concentrations of 0.0, 0.5, 1.0, 1.5, 2.0, and 2.5 wt%. Fig. 4(a) displays the stress and viscosity *versus* shear rate at 190 °C, indicating that when the stress increases, the viscosity decreases, whereas in Fig. 4(b), there are MFR levels at 190 °C, indicating that as the filler increases, the MFR levels decrease.

Fig. 5 presents the thermal characteristics of the PHA/biochar (0.0, 0.5, 1.0, 1.5, 2.0, and 2.5 wt%) composite samples. In particular, Fig. 5(a) is related to TGA, as it shows weight *versus* temperature graphs, while the respective values of the initial decomposition temperature (IDT) and final residue (FR) are provided in the bar chart of Fig. 5(d). Their maximum values were detected at PHA/2.5 wt% biochar and pure PHA, respectively. Fig. 5(b) shows the DSC results of the heat flow *versus* temperature graphs, accompanied by the measured T_m values shown in Fig. 5(c). This indicated that the highest T_m value was that of pure PHA.

3.3. DMA results and mechanical properties

Fig. 6 presents the DMA-derived data, including graphs of the loss modulus, storage modulus, and tan(δ) with respect to temperature for the following samples: pure PHA (Fig. 6(a)), PHA/biochar composites with content per weight of 0.5 (Fig. 6(b)), 1.0 (Fig. 6(c)), 1.5 (Fig. 6(d)), 2.0 (Fig. 6(e)), and 2.5 (Fig. 6(f)). There are also bars representing the bending modulus of elasticity to be compared with the respective storage modulus, as it was derived at room temperature. As the storage modulus and loss modulus decrease, tan(δ) increases until it reaches the T_m value, after which it decreases.

Fig. 7 presents the tensile test results for the PHA/biochar specimens with filler concentrations of 0.0, 0.5, 1.0, 1.5, 2.0, and 2.5 wt%. Fig. 7(a) presents the tensile strength values and an illustration acquired during the tensile experiment of a randomly selected example. Notably, the sample with the highest tensile strength belongs to 1.0 wt%, with a 15.3% increase compared to pure PHA. Fig. 7(b) shows the Young modulus results and the failed tensile specimen from the 1.0 wt% composite, which again demonstrated the highest value (25.4% above pure PHA). The tensile toughness results are presented in Fig. 7(c), along with an image of the failed tensile specimen from the PHA/0.5 wt% biochar composite, with this formulation featuring the highest toughness (17.7% above pure PHA). Additionally, in the tan(δ) curves, two distinct peaks of relaxation can be observed, which can be attributed to the interfacial phenomena appearing when the biochar content is included in the polymer matrix.

Fig. 8 displays the bending test results for the 3D-printed PHA/biochar specimens with filler concentrations of 0.0, 0.5, 1.0, 1.5, 2.0, and 2.5 wt%. Fig. 8(a) shows the bending strength values accompanied by a picture of the bending test of a randomly selected specimen. The 0.5 wt% composite exhibited the highest bending strength, achieving a 15.3% increase compared to pure PHA. Fig. 8(b) shows the bending modulus of elasticity and an image of a pure PHA-failed bending specimen. None of the PHA/biochar composite formulations reached a value higher than that of pure PHA. The bending toughness results are presented in Fig. 8(c), along with an image from the PHA/0.5 wt% biochar bending specimen after it failed. Regarding the highest tensile toughness, the case of 0.5 wt% reveals a 3.1% higher value than that of pure PHA.

Fig. 9(a) shows the tensile toughness of the fabricated PHA/biochar (0.0, 0.5, 1.0, 1.5, 2.0, and 2.5 wt%) filaments and a picture taken during the tensile testing of a randomly chosen filament sample. The highest tensile toughness was achieved for the pure PHA. As the biochar filler concentration increased,

Table 2 Differences in the major Raman peaks of PHA/biochar from the unfilled PHA

60	Decrease	Small decrease in Raman peak intensity
81	Increase	Medium increase of Raman peak intensity
447	Decrease	Small decrease in Raman peak intensity
611	Decrease	Small decrease of C–COO vibration, C–C–O symmetric vibration
841	Increase	Medium increase of phenyl ring vibration
1727	Increase	Small increase of C═O
2930	Gradual increase	Strong increase of CH_2 asymmetric stretching; CH vibration, with a maximum at 20 and 25 wt%
2974	Gradual increase	Small increase of C–H stretching, with a maximum at 20 and 25 wt%
3000	Gradual increase	Small increase of C–H stretching, with a maximum at 20 and 25 wt%

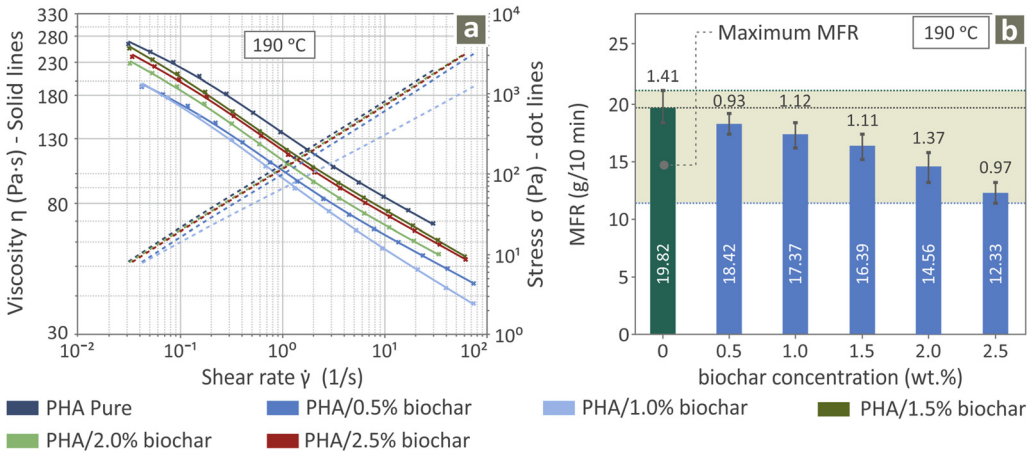

Fig. 4 Rheology results for PHA/biochar (0.0, 0.5, 1.0, 1.5, 2.0, and 2.5 wt%) composite samples (a) stress and viscosity *versus* shear rate results and (b) MFR levels.

toughness decreased. Additional filament testing, as well as the results from diameter monitoring and related captured images, are shown in the ESI.† Fig. 9(b) shows the Charpy impact strength of PHA/biochar (0.0, 0.5, 1.0, 1.5, 2.0, and 2.5 wt%)

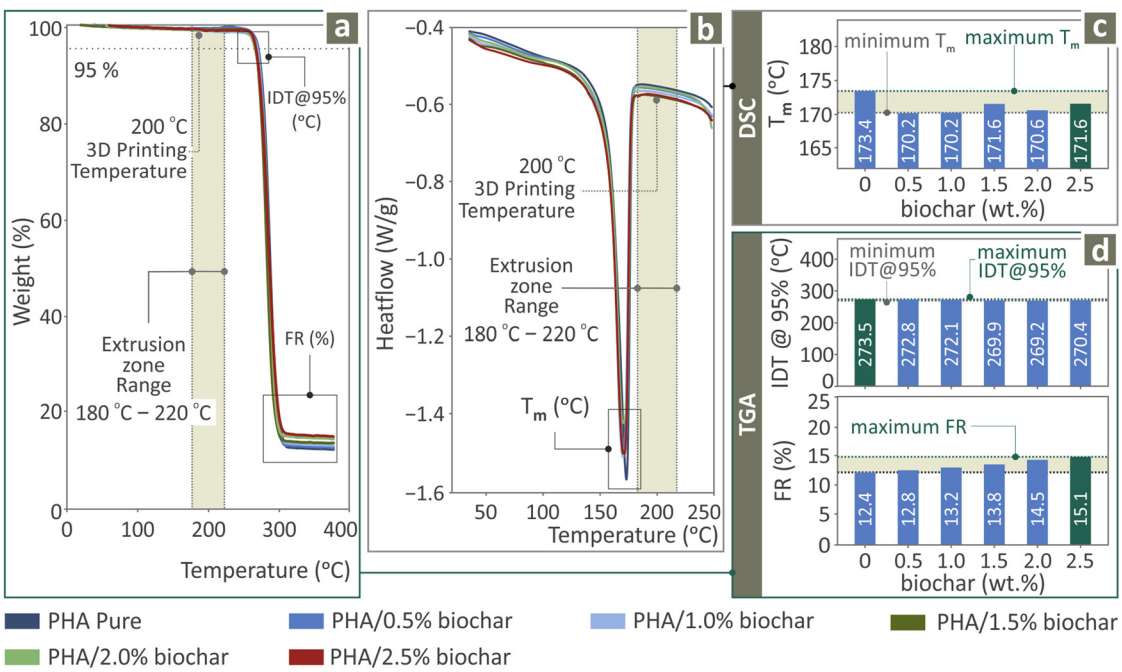

Fig. 5 Thermal property results of pure PHA and PHA/biochar (0.0, 0.5, 1.0, 1.5, 2.0, and 2.5 wt%) composite samples through (a) TGA and (b) DSC curves, as well as the respective measured (c) T_m, (d) FR, and IDT values.

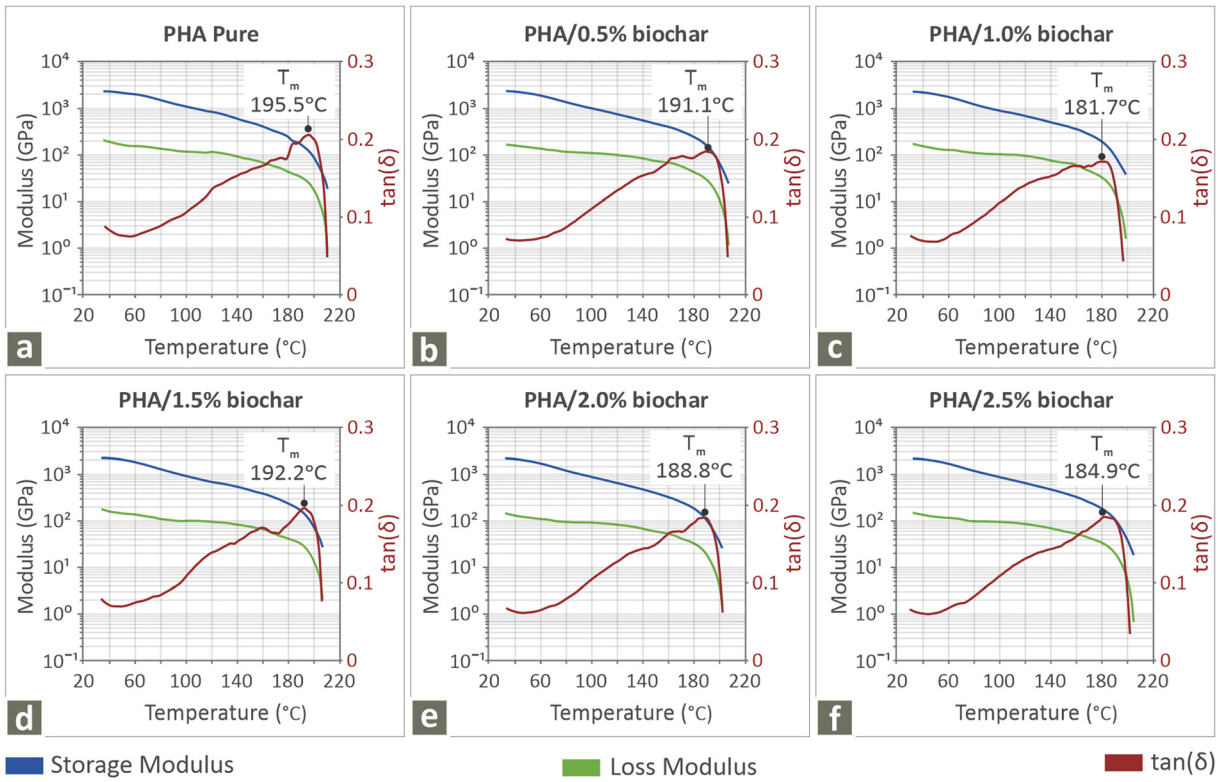

Fig. 6 DMA results in terms of storage modulus, loss modulus, and tan(δ) *vs.* temperature graphs for (a)–(f) PHA/biochar concentrations of 0.0, 0.5, 1.0, 1.5, 2.0, and 2.5 wt%, respectively.

samples, along with an image of a Charpy PHA/0.5 wt%. biochar specimen. The highest levels were detected in the PHA/0.5 wt% biochar, as its values were increased by1.9% compared to the unfilled PHA. Fig. 9(c) depicts the microhardness (M–H) values of all the PHA/biochar samples and an image showing the Vickers imprint of a PHA pure sample. The highest M–H values were obtained for pure PHA, which declined as the biochar particle content increased. The tensile stress *vs.* strain graphs of the specimens and filaments and the bending stress *vs.* strain graphs of the filaments are presented in the ESI.†

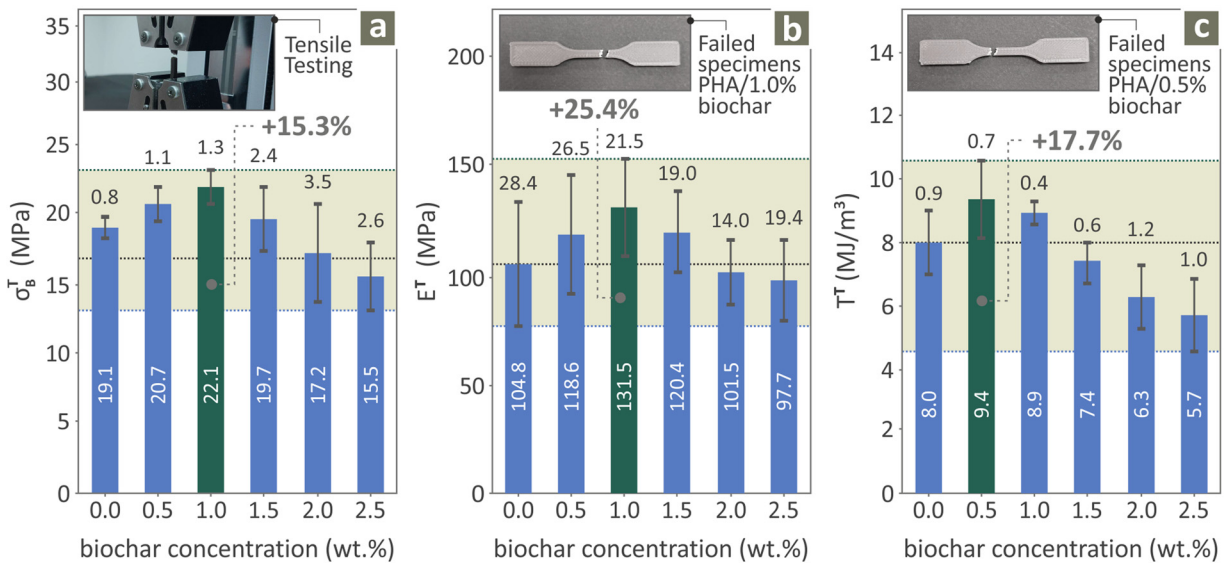

Fig. 7 Tensile results for the 3D-printed PHA/biochar (0.0, 0.5, 1.0, 1.5, 2.0, and 2.5 wt%) specimens: (a) tensile strength and an image from the tensile testing of a randomly selected specimen, (b) tensile modulus of elasticity and an image from a PHA/1.0 wt% biochar failed tensile specimen, and (c) tensile toughness, and an image from a PHA/0.5 wt% biochar failed tensile specimen.

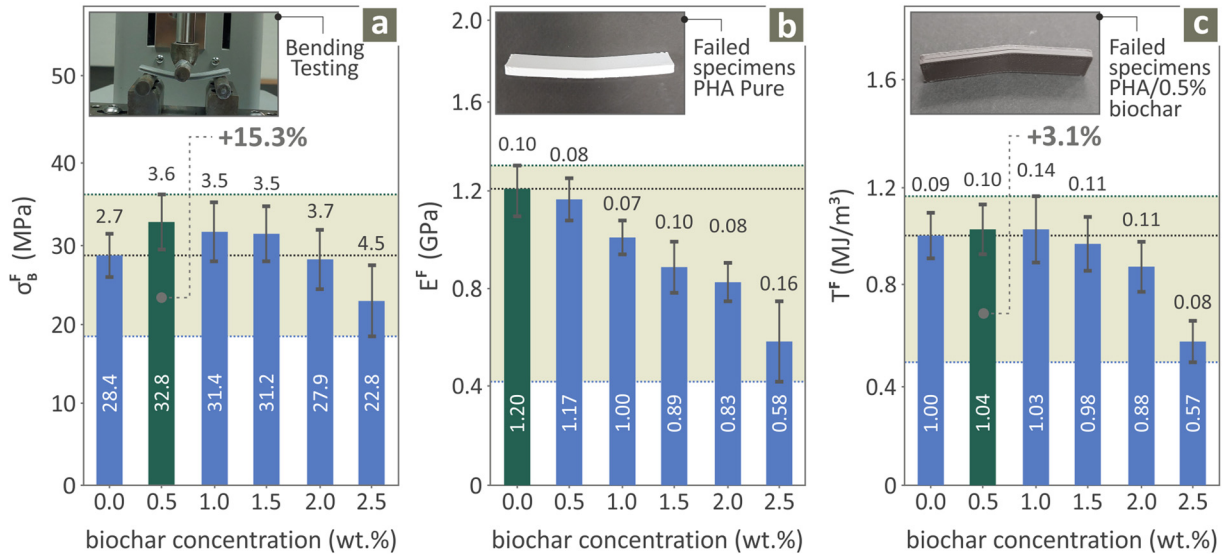

Fig. 8 Results from the bending 3D-printed PHA/biochar (0.0, 0.5, 1.0, 1.5, 2.0, and 2.5 wt%) specimens; (a) bending strength and an image from the bending testing of a randomly selected specimen, (b) bending modulus of elasticity and an image from a pure PHA failed tensile specimen, and (c) bending toughness and an image from a PHA/0.5 wt% biochar failed to bend the specimen.

3.4. μ-CT results

Fig. 10 shows the geometrical deviation results for the fabricated PHA/biochar specimens. Fig. 10(a) and (b) show the dimensional deviation through color-coded mapping of a PHA/0.5 wt% biochar tensile sample. As shown in Fig. 10(c), the actual to nominal geometry (A2N) at 95% (5% of the extreme were ignored) dimensional deviation levels of the PHA/biochar composites for all filler concentrations (0.0, 0.5, 1.0, 1.5, 2.0, and 2.5 wt%) is depicted. The lowest deviation was detected in the case of 1.0 wt%, which is 11.2% lower than that of the pure PHA; that is, the sample is closer to the nominal dimensions by 11.2% compared to the pure PHA. Fig. 10(d) and (e) show a section of the PHA/0.5 wt% biochar sample through color-coded mapping. Fig. 10(f) presents the porosity levels of all PHA/biochar samples and highlights that the lowest porosity levels were detected in the case of 1.0 wt%, a value that is 23.3% lower (less porous structure) than in the pure PHA. Additional information derived from the structural investigation of the specimens is shown in the ESI.†

3.5. SEM-assisted morphological characterization

Fig. 11 and 12 present the SEM illustrations of selected PHA/biochar specimens (tensile) captured at various magnifications, showing various lateral and fractured surfaces. In Fig. 11(a)–(c), SEM images of the unfilled PHA are depicted, indicating the vertical side

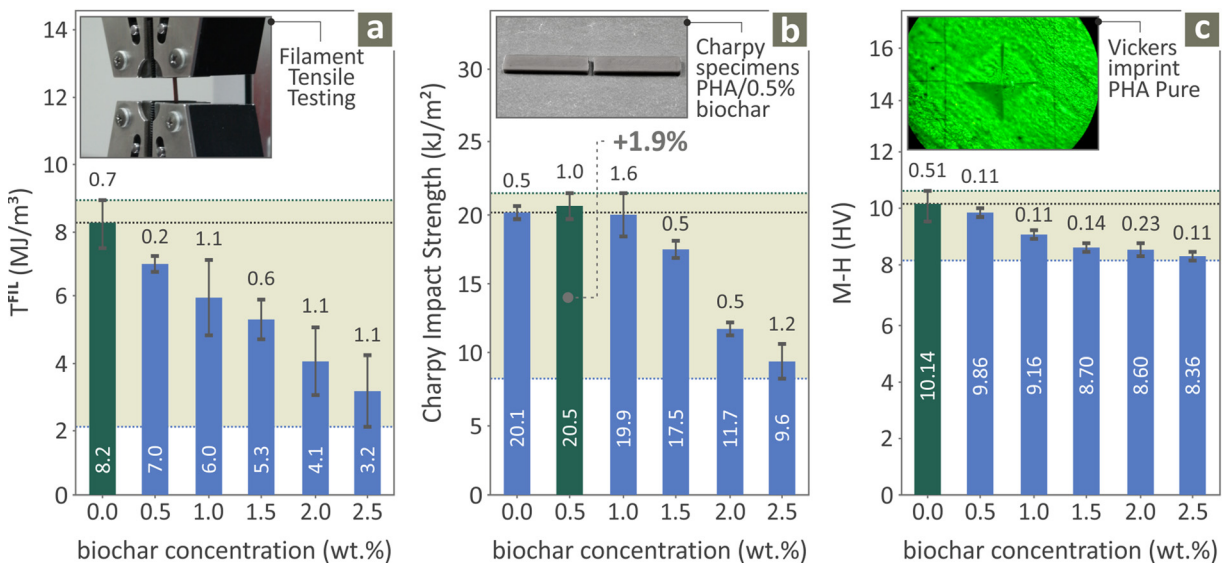

Fig. 9 Mechanical characterization results of PHA/biochar samples for all filler concentrations, to derive: (a) tensile toughness of the extruded filaments, (b) Charpy impact strength of the 3D-printed specimens, and (c) microhardness.

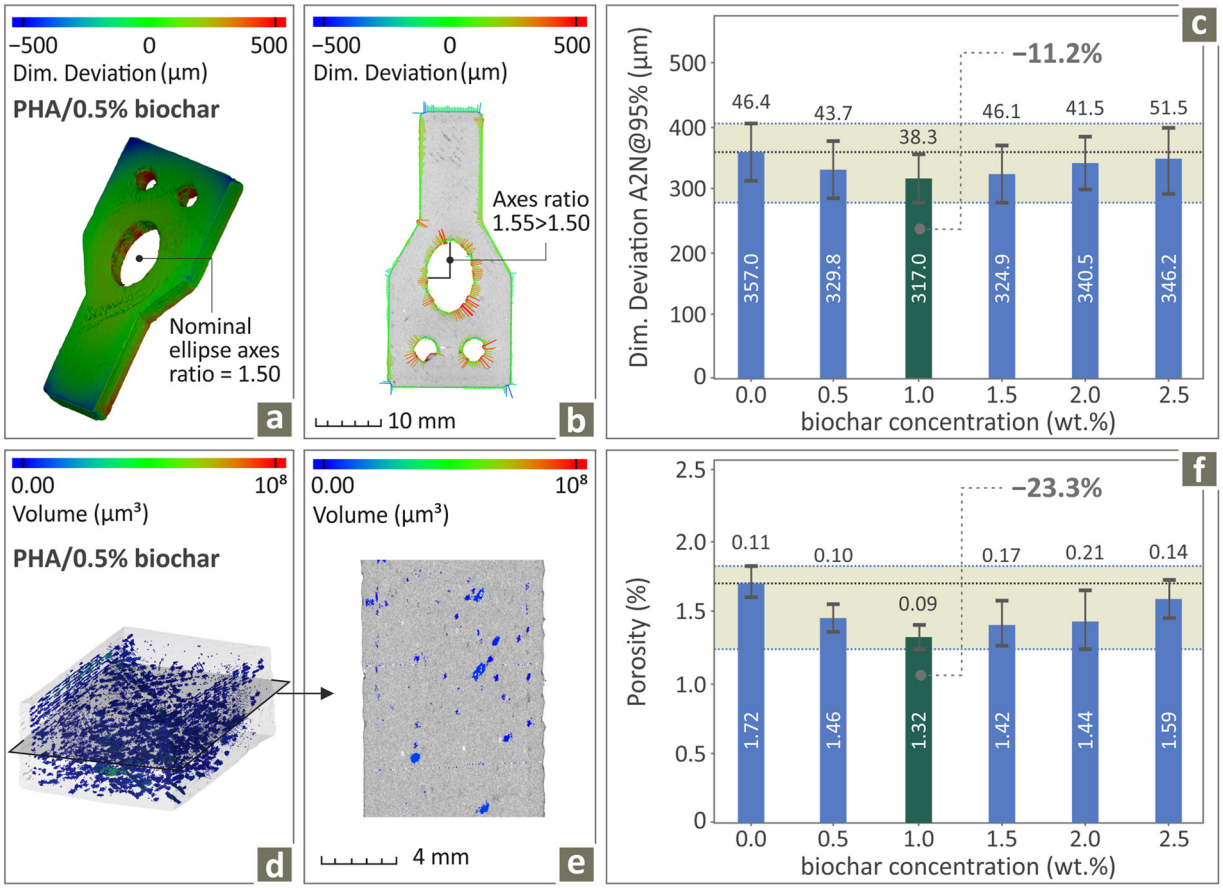

Fig. 10 (a) and (b) Dimensional deviation of a PHA/0.5 wt% biochar example through color-coded mapping, (c) geometrical accuracy values of all PHA/biochar samples, (d), (e) PHA/0.5 wt% biochar section through color-coded mapping, and (f) porosity values of all PHA/biochar samples.

magnified at 150× and the fractured section at both 27× and 20 000×. In Fig. 11(d)–(f) and in Fig. 11(g)–(i), corresponding information is provided for PHA/1.0 wt% biochar and PHA/2.0 wt% biochar. Fig. 12 shows the SEM pictures of the PHA/1.5 wt% biochar; the vertical surface magnified at 27× (Fig. 12(a)), as well as the fractured surface magnified at 27× (Fig. 12(b)), 1000× (Fig. 12(d)), 5000× (Fig. 12(e)), and 20 000× (Fig. 12(f)). Additionally, Fig. 12(c) shows the distribution of C, O, and Si in the PHA/1.5 wt% biochar composite is presented. Considering the lateral surface images, 3D-printing layering was characterized by a defect-free uniform distribution across all examined samples. The images of the fractured surfaces revealed that all the examined samples exhibited ductile behavior (deformation of the strands before their failure is evident), except for PHA/2.0 wt% biochar, which shows brittle fracture characteristics (minimum deformation is presented on the fracture surface).

4. Discussion

The evaluation of the test results revealed several observations. Pure PHA was proven to exhibit the highest performance in terms of the bending modulus of elasticity, microhardness, and filament tensile toughness. The rest of the mechanical properties were most enhanced for the compounds with values of biochar particle content per weight of 0.5 and 1.0. Specifically, the 0.5 wt% composite demonstrated superior tensile and bending toughness, bending strength, and Charpy impact strength. The 1.0 wt% composite achieved the most improved tensile strength and Young modulus. At the same time, it was characterized by the lowest dimensional deviation and porosity relative to pure PHA. It can be observed that the toughness decreases in the tensile test for compounds with the biochar content beyond the one that achieved the highest strength (1 wt%). This shows that beyond this loading, the mechanical properties overall decline. Also, it is an indication that the parts are becoming more brittle at a higher loading (fail at lower strain), as the toughness depends on both strength and strain. It is also notable that the flexural modulus of elasticity decreases with the introduction of biochar in the PHA, meaning that the samples are becoming less stiff in this type of loading, with the addition of biochar. This is not the case with tensile strength, in which the stiffness of the samples increases by a notable 25.4% (1 wt%). It should also be noted that the flexural modulus of elasticity is in good agreement with the storage modulus derived from the DMA measurement at room temperature.

The toughness of the samples in the flexural test is rather stable (differences are within the statistical error), which is

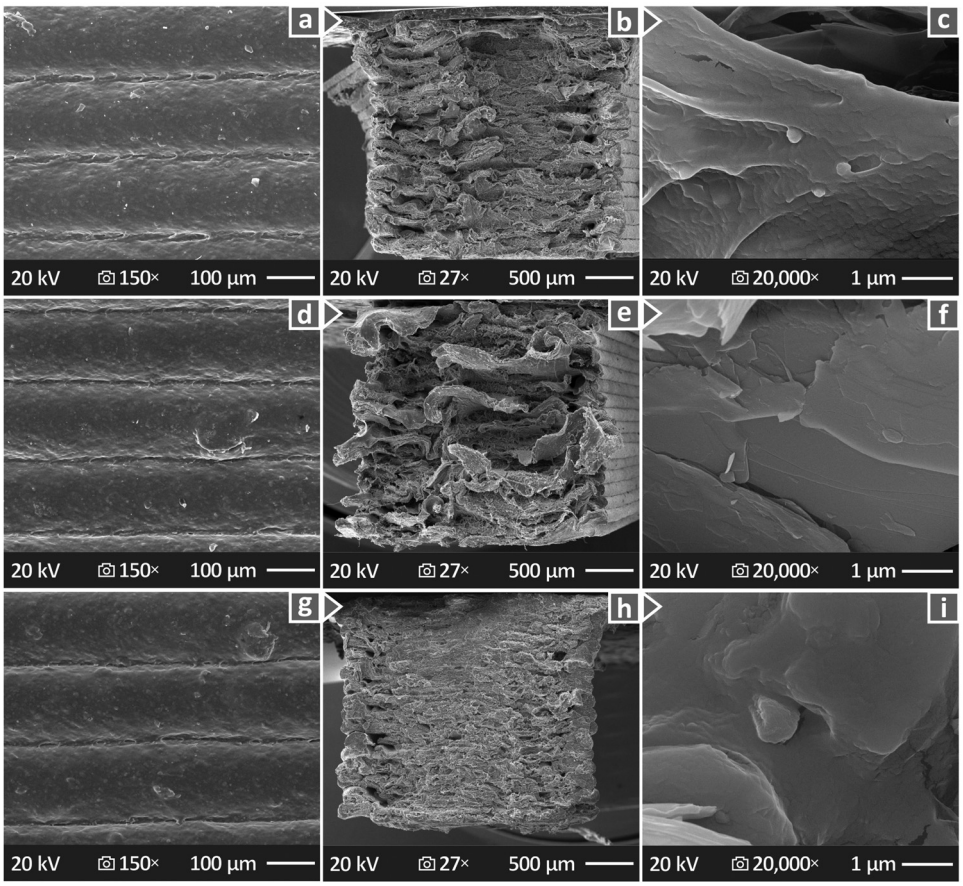

Fig. 11 SEM images showing (a)–(c) unfilled PHA, (d)–(f) PHA/1.0 wt% biochar and (g)–(i) PHA/2.0 wt% biochar: lateral surfaces at 150× magnification, and fractured surfaces at 27× and 20 000×.

probably due to the termination of the tests at 5% strain in the experiment, in accordance with the standard instructions. At higher loadings, the toughness decreased in the flexural test. On the tensile tests of the filament, the toughness constantly

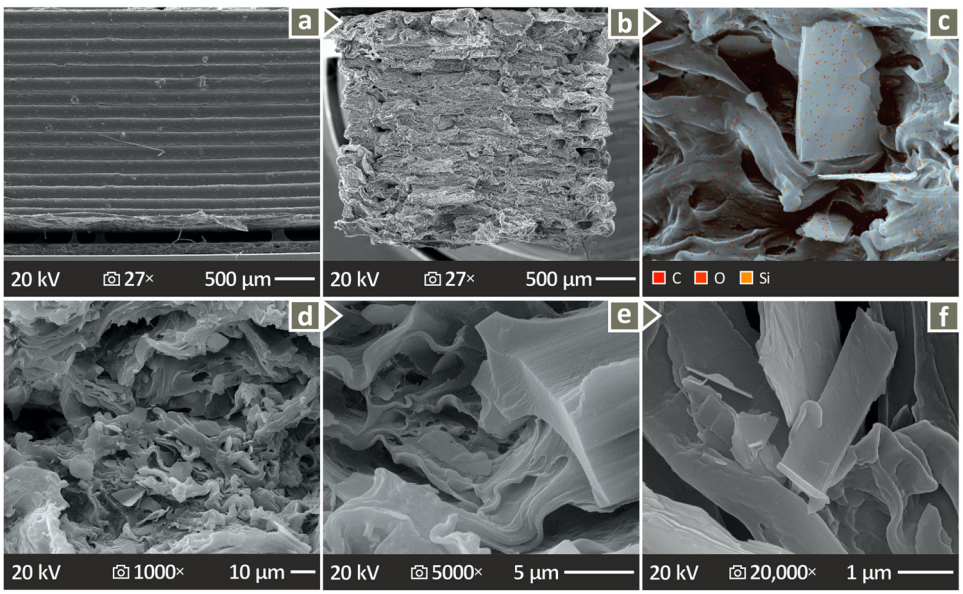

Fig. 12 SEM images of the PHA/1.5 wt% biochar: (a) lateral surface magnified at 27×, (b) vertical surface magnified 27×, (c) C, O, and Si elemental distribution through EDS, and (d)–(f) side surface magnified 1000×, 5000×, and 20 000×.

decreased, despite the increase in the strength of up to 1.5 wt%. This shows that the filament is more brittle with the introduction of the biochar in the PHA biopolymer. The impact strength is also rather stable (differences are within the statistical error) and decreased at a higher biochar loading in the compounds. M–H also decreased with the introduction of biochar in the PHA biopolymer, showing that biochar failed to improve the hardness of the compounds. In Fig. 13, spider-shaped graphs summarize the tensile and bending strengths, dimensional deviation, and porosity values, while the maximum and minimum values relevant to this research work are also highlighted.

Regarding thermal properties, the IDT was stable with differences within statistical error for all the compounds, showing that the introduction of the biochar in the PHA biopolymer does not alter its thermal response. The FR increased as expected with the increase of the biochar content in the compounds. Regarding the T_m, DSC showed that it was not affected by the addition of biochar (differences are within the statistical error). On the other hand, DMA showed a decrease in the T_m of the PHA with the addition of biochar; T_m measurements with DMA are considered more reliable.

The MFR decreased with an increase in biochar content; that is, higher filler amounts resulted in lower MFR values. Higher MFR values indicate that the addition of biochar makes PHA easier to process. Still, the effect of the addition of biochar on the rheology of the PHA polymer should be evaluated against the 3D printing settings, which probably would require adjustments as the MFR increases. By inspecting the lateral surfaces of the tensile samples with SEM, the quality is not diminished with the increase of the biochar content. So, this assumption (need for 3D printing alteration due to different rheology in the compounds) probably does not stand in this case. Still, differences in the structure of the parts (porosity and dimensional accuracy) were found in the μ-CT scan process, which can be attributed, among others, to the impact of biochar on the rheological properties of the compounds. Moreover, since both the MFR and the viscosity decreased, this is typically an indication that the polymer might be experiencing shear-thinning behavior or specific interactions with the biochar.

Regarding the evaluation of the 3D printing structure, as mentioned above, differences were found. The introduction of biochar enhanced both the geometrical accuracy and the porosity in the structure of the 3D-printed samples for all concentrations considered in the research. Interestingly enough, the best values were found for the 1 wt% compound, the one with the highest response in the tensile test, showing a correlation between these two (related to the structure) qualities and the 3D printed items' mechanical response.

The SEM images revealed a high-quality and uniform layer distribution, as well as ductile behavior in pure PHA, PHA/1.0 wt% biochar and PHA/1.5 wt% biochar composites, and a brittle behavior for the PHA/2.0 wt% biochar compound. The more brittle response of the higher-loaded compounds mentioned above (evaluated by the toughness findings) was verified in the SEM images. Furthermore, the dispersion of the elements determined by the EDS revealed good dispersion of the biochar particles, which is a positive outcome for the methodology followed for the preparation of the composites.

To the best of the authors' knowledge, no previous investigation has produced and characterized bio-composite PHA/biochar filaments and corresponding 3D-printed specimens in this manner. However, the scientific community has been

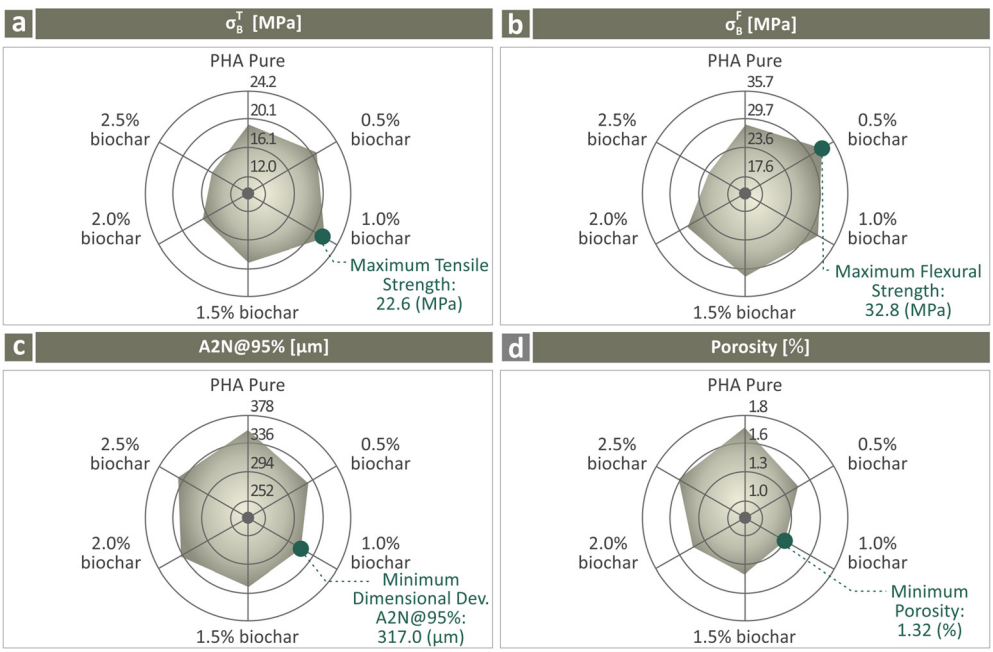

Fig. 13 Spider-shaped graphs, with regard to all the PHA/biochar samples for (a) tensile and (b) flexural strength, (c) dimensional deviation, and (d) porosity.

Table 3 Biochar efficacy as a reinforcing agent in MEX 3D AM for common polymers and the PHA biopolymer

Increase (%)	PHA	PLA[107]	PP[108]	ABS[109]	HDPE[110]
Tensile strength	15.3	20.9	28.4	24.9	37.8
Young modulus	25.4	25.8	24.3	25.5	29.5
Flexural strength	15.3	14.1	19.7	21.0	35.9
Opt. loading (wt%)	1.0	4.0	4.0	4.0	6.0

involved in exploring other biocomposite systems for application in 3D printing.[125,126] Still, as mentioned in the Introduction section, conventional, non-degradable polymers have been used for the development of composites in the MEX AM method with biochar particles as fillers. These specific research studies mentioned, furthermore, used the same biochar grade, and the composites were fabricated using techniques similar to those employed in the current research. No other additives were used in all cases. A summary of mechanical properties from the existing literature is presented in Table 3, in which the differences in the reinforcement effect of the specific biochar grade on different polymers are presented and compared with the current research findings of the PHA biopolymer. The last row of Table 3 states the optimum biochar amount (wt%) found in each compound. The improvement achieved with this optimum biochar amount in each compound is stated in the other rows of the table, which state the % improvement in different mechanical properties, compared to the respective unfilled polymer used as a matrix material in each compound. As shown, the biochar amount that achieved the best results differs in each compound (different matrix material). This can be attributed to the different interactions between biochar and each polymeric matrix. Also, it justifies the need for individual studies for each matrix/biochar combination. It should be noted also that in these studies, apart from the same biochar used, the composite preparation method was similar to the current research.

As shown, the findings of the current research are similar to those for the PLA polymer.[107] The reinforcing effect on the other polymers is higher than that of PHA. Still, the differences are not that high. This is an important outcome, considering the nature-sourced character of the PHA biopolymer. Additionally, it can be observed that the optimum loading for all conventional, non-degradable polymers was higher than the PHA biopolymer. For the PHA biopolymer, a further increase in the biochar content triggered processability issues, making the preparation of the samples more difficult.

5. Conclusions

In the present research, biocomposites of naturally produced PHA and biochar from biomass were fabricated, characterized, and tested in biochar compositions of 0.0, 0.5, 1.0, 1.5, 2.0, and 2.5 wt%. The created mixtures were then extruded into filaments, which were employed for the 3D printing of the desired examples. Subsequently, the rheology, thermal, and mechanical characteristics, structure, morphology, and chemical composition of the specimens were examined. Rheological analysis provided data on the viscosity and melt flow rate, while thermal characterization included TGA and DSC measurements, yielding the FR, IDT, and T_m values. Dynamic mechanical analysis was also performed, along with assessments of the tensile and bending strength, modulus of elasticity, and toughness. Furthermore, the impact strength (Charpy notched) and Vickers M–H were measured, and the tensile properties of the filaments were evaluated. The structural analysis of the 3D-printed examples involved dimensional deviation and porosity measurements. Finally, a morphological investigation was performed using SEM on both the lateral and fractured surfaces at various magnifications, and EDS was employed to determine the elemental composition of the samples.

Based on mechanical and structural analyses, the PHA/biochar composites with 0.5 and 1.0 wt% filler displayed the best overall performance. Notably, the 0.5 wt% composite presented a tensile toughness that was 17.7% higher than that of pure PHA, whereas the 1.0 wt% composite showed a Young modulus of 25.4% improved compared to the unfilled PHA. Additionally, the 23.3% lower porosity of the PHA/1.0 wt% biochar composite samples constitute an important improvement for the 3D printing structure (and by extension to the quality of the part) compared to pure PHA. The incorporation of biochar into PHA was proven to improve the performance of the compound, suggesting its potential in applications that require such properties. Future work could include investigation of the same composites from a ''3D printing parameter optimization'' perspective to further improve and tailor their properties. Furthermore, different types of biochar can be evaluated to derive conclusions regarding the effect of the grade on the efficacy of the composites. Extra tests can be carried out, such as additional rheology tests (temperature-dependent sweeps or applying rheological models such as the power-law or Carreau–Yasuda model). Finally, creating an actual complex-shaped part with 0.5 and 1 wt% biochar and then comparing it with the 0 wt% biochar case could provide useful insight into the performance of the composites in real-life applications.

Author contributions

Nectarios Vidakis: conceptualization, methodology, resources, supervision, and project administration; Nikolaos Michailidis: supervision and project administration; Dimitrios Kalderis: investigation, methodology, validation, and formal analysis; Apostolos Argyros: data curation and visualization; Nikolaos Mountakis: formal analysis, data curation, and visualization; Maria Spyridaki: writing – original draft preparation and investigation; Ioannis Valsamos: formal analysis and data curation; Vassilis Papadakis: visualization and validation; and Markos Petousis: methodology, formal analysis, writing – original draft preparation, and writing – review and editing. The manuscript was written with the contributions of all authors. All authors have approved the final version of the manuscript.

Conflicts of interest

The authors declare no conflicts of interest.

Data availability

The authors confirm that the data supporting the findings of this study are available within the article and its ESI.†

Acknowledgements

The authors would like to thank the Institute of Electronic Structure and Laser of the Foundation for Research and Technology-Hellas (IESL-FORTH) and, in particular, Ms Aleka Manousaki for taking the SEM images presented in this work, and the Photonic Phononic and Meta-Materials Laboratory for sharing the Raman Instrumentation. This research was partially supported by the academic fellowship of an HMU post-doctoral research program in 2022, Greece.

References

1 A. Kumar and T. Bhattacharya, Biochar: a sustainable solution, *Environ. Dev. Sustain.*, 2021, **23**, 6642–6680.
2 M. Kumar, R. Rathour, R. Singh, Y. Sun, A. Pandey, E. Gnansounou, K.-Y. Andrew Lin, D. C. W. Tsang and I. S. Thakur, Bacterial polyhydroxyalkanoates: Opportunities, challenges, and prospects, *J. Cleaner Prod.*, 2020, **263**, 121500.
3 R. Tiwari, N. Azad, D. Dutta, B. R. Yadav and S. Kumar, A critical review and future perspective of plastic waste recycling, *Sci. Total Environ.*, 2023, **881**, 163433.
4 K. K. Khoaele, O. J. Gbadeyan, V. Chunilall and B. Sithole, The Devastation of Waste Plastic on the Environment and Remediation Processes: A Critical Review, *Sustainability*, 2023, **15**, 5233.
5 M. Mehrpouya, H. Vahabi, M. Barletta, P. Laheurte and V. Langlois, Additive manufacturing of polyhydroxyalkanoates (PHAs) biopolymers: Materials, printing techniques, and applications, *Mater. Sci. Eng., C*, 2021, **127**, 112216.
6 D. F. Lekkas, I. Panagiotakis and D. Dermatas, A digital circular bioeconomy – Opportunities and challenges for waste management in this new era, *Waste Manage. Res.*, 2021, **39**, 407–408.
7 M. Shahbazi and H. Jäger, Current Status in the Utilization of Biobased Polymers for 3D Printing Process: A Systematic Review of the Materials, Processes, and Challenges, *ACS Appl. Bio Mater.*, 2021, **4**, 325–369.
8 Spherical Insights, Global Bio-Based Chemicals Market Size To Exceed USD 177.0 Billion By 2033: Market Growth Report, **https://www.sphericalinsights.com/our-insights/bio-based-chemicals-market**, (accessed 5 July 2025).
9 European Bioplastics, Bioplastics market development update 2024, **https://www.european-bioplastics.org/market/**, (accessed 5 July 2025).
10 A. Papacharalampopoulos, K. Tzimanis and P. Stavropoulos, A decision support tool for dynamic LCA: the FDM paradigm, *Proc. CIRP*, 2022, **112**, 543–548.
11 J. Kluczyński, K. Jasik, J. Łuszczek, B. Sarzyński, K. Grzelak, T. Dražan, Z. Joska, I. Szachogłuchowicz, P. Płatek and M. Małek, A Comparative Investigation of Properties of Metallic Parts Additively Manufactured through MEX and PBF-LB/M Technologies, *Materials*, 2023, **16**, 5200.
12 P. Stavropoulos and P. Foteinopoulos, Modelling of additive manufacturing processes: a review and classification, *Manuf. Rev.*, 2018, **5**, 2.
13 S. El-Sayegh, L. Romdhane and S. Manjikian, A critical review of 3D printing in construction: benefits, challenges, and risks, *Arch. Civ. Mech. Eng.*, 2020, **20**, 34.
14 H. S. Far, M. Najafi, M. Hasanzadeh and M. Rabbani, Self-Supported 3D-Printed Lattices Containing MXene/Metal–Organic Framework (MXOF) Composite as an Efficient Adsorbent for Wastewater Treatment, *ACS Appl. Mater. Interfaces*, 2022, **14**, 44488–44497.
15 Z. Zhou, K. Xu, C. Li, J. Lin, J. Bian, K. Sun, J. Jiang, S.-F. Zhou and G. Zhan, Assembly of 3D printed N-doped biochar as impeller with $CaCO_3$ as sacrificial pore generator for enhanced dye adsorption, *Chem. Eng. J.*, 2024, **497**, 154661.
16 E. MacDonald and R. Wicker, Multiprocess 3D printing for increasing component functionality, *Science*, 2016, **353**, aaf2093.
17 R. Allouzi, W. Al-Azhari and R. Allouzi, Conventional Construction and 3D Printing: A Comparison Study on Material Cost in Jordan, *J. Eng.*, 2020, **2020**, 1–14.
18 B. A. Praveena, N. Lokesh, A. Buradi, N. Santhosh, B. L. Praveena and R. Vignesh, A comprehensive review of emerging additive manufacturing (3D printing technology): Methods, materials, applications, challenges, trends and future potential, *Mater. Today: Proc.*, 2022, **52**, 1309–1313.
19 M. N. Nadagouda, M. Ginn and V. Rastogi, A review of 3D printing techniques for environmental applications, *Curr. Opin. Chem. Eng.*, 2020, **28**, 173–178.
20 M. S. Karkun and S. Dharmalinga, 3D Printing Technology in Aerospace Industry – A Review, *Int. J. Aviat. Aeronaut. Aerosp.*, 2022, **9**(2), 4.
21 Z. Wawryniuk, E. Brancewicz-Steinmetz and J. Sawicki, Revolutionizing transportation: an overview of 3D printing in aviation, automotive, and space industries, *Int. J. Adv. Des. Manuf. Technol.*, 2024, **134**, 3083–3105.
22 N. Nachal, J. A. Moses, P. Karthik and C. Anandharamakrishnan, Applications of 3D Printing in Food Processing, *Food Eng. Rev.*, 2019, **11**, 123–141.
23 A. Aimar, A. Palermo and B. Innocenti, The Role of 3D Printing in Medical Applications: A State of the Art, *J. Healthc. Eng.*, 2019, **2019**, 1–10.
24 S. Kholgh Eshkalak, E. Rezvani Ghomi, Y. Dai, D. Choudhury and S. Ramakrishna, The role of three-dimensional printing in healthcare and medicine, *Mater. Des.*, 2020, **194**, 108940.
25 S. S. L. Chan, R. M. Pennings, L. Edwards and G. V. Franks, 3D printing of clay for decorative architectural

applications: Effect of solids volume fraction on rheology and printability, *Addit. Manuf*, 2020, **35**, 101335.
26 N. Shahrubudin, T. C. Lee and R. Ramlan, An Overview on 3D Printing Technology: Technological, Materials, and Applications, Procedia Manuf, *Procedia Manuf.*, 2019, **35**, 1286–1296.
27 A. H. Espera, J. R. C. Dizon, Q. Chen and R. C. Advincula, 3D-printing and advanced manufacturing for electronics, *Prog. Addit. Manuf.*, 2019, **4**, 245–267.
28 A. M. E. Arefin, N. R. Khatri, N. Kulkarni and P. F. Egan, Polymer 3D Printing Review: Materials, Process, and Design Strategies for Medical Applications, *Polymers*, 2021, **13**, 1499.
29 N. Vidakis, M. Petousis, I. Ntintakis, C. David, D. Sagris, N. Mountakis and A. Moutsopoulou, Quantitative Insight into the Compressive Strain Rate Sensitivity of Polylactic Acid, Acrylonitrile Butadiene Styrene, Polyamide 12, and Polypropylene in Material Extrusion Additive Manufacturing, *J. Dyn. Behav. Mater.*, 2024, **10**, 251–269.
30 Z. Chen, Z. Li, J. Li, C. Liu, C. Lao, Y. Fu, C. Liu, Y. Li, P. Wang and Y. He, 3D printing of ceramics: A review, *J. Eur. Ceram. Soc.*, 2019, **39**, 661–687.
31 C. Buchanan and L. Gardner, Metal 3D printing in construction: A review of methods, research, applications, opportunities and challenges, *Eng. Struct.*, 2019, **180**, 332–348.
32 I. Blanco, The Use of Composite Materials in 3D Printing, *J. Compos. Sci.*, 2020, **4**, 42.
33 M. Petousis, V. Papadakis, A. Moutsopoulou, M. Spiridaki, A. Argyros, E. Sfakiotakis, N. Michailidis, E. Stratakis and N. Vidakis, The effect of Hydroxyapatite particle shape, and concentration on the engineering performance and printability of Polycaprolactone-Hydroxyapatite composites in Bioplotting, *Bioprinting*, 2024, e00370.
34 N. Michailidis, M. Petousis, A. Moutsopoulou, A. Argyros, I. Ntintakis, V. Papadakis, N. K. Nasikas and N. Vidakis, Engineering response of biomedical grade isotactic polypropylene reinforced with titanium nitride nanoparticles for material extrusion three-dimensional printing, *Eur. J. Mater.*, 2024, **4**, 1–24.
35 N. Vidakis, V. Saltas, C. David, D. Sagris, N. K. Nasikas, N. Mountakis, M. Spiridaki and M. Petousis, Interpretation of MEX additive manufacturing generic control settings impact on the spatial dielectric response of ABS: challenges and opportunities for the defense industry, *Int. J. Interact. Des. Manuf.*, 2024, **19**, 5491–5523.
36 N. Vidakis, M. Petousis, N. Mountakis, V. Papadakis, C. Charou, V. Rousos and P. Bastas, Glass Fillers in Three Different Forms Used as Reinforcement Agents of Polylactic Acid in Material Extrusion Additive Manufacturing, *Appl. Sci.*, 2023, **13**(11), 6471.
37 N. K. Nasikas, M. Petousis, V. Papadakis, A. Argyros, J. Valsamos, K. Gkagkanatsiou, D. Sagris, C. David, N. Michailidis, E. Maravelakis and N. Vidakis, A Comprehensive Optimization Course of Antimony Tin Oxide Nanofiller Loading in Polyamide 12: Printability, Quality Assessment, and Engineering Response in Additive Manufacturing, *Nanomaterials*, 2024, **14**, 1285.
38 N. Michailidis, M. Petousis, V. Saltas, V. Papadakis, M. Spiridaki, N. Mountakis, A. Argyros, J. Valsamos, N. K. Nasikas and N. Vidakis, Investigation of the Effectiveness of Silicon Nitride as a Reinforcement Agent for Polyethylene Terephthalate Glycol in Material Extrusion 3D Printing, *Polymers*, 2024, **16**, 1043.
39 N. Cakir Yigit and I. Karagoz, A review of recent advances in bio-based polymer composite filaments for 3D printing, *Polym.-Plast. Technol. Mater.*, 2023, **62**, 1077–1095.
40 K. Zhang, L. Ketterle, T. Järvinen, S. Hong and H. Liimatainen, Conductive hybrid filaments of carbon nanotubes, chitin nanocrystals and cellulose nanofibers formed by interfacial nanoparticle complexation, *Mater. Des.*, 2020, **191**, 108594.
41 R. Mandala, A. P. Bannoth, S. Akella, V. K. Rangari and D. Kodali, A Short Review on Fused Deposition Modeling 3D Printing of Bio-based Polymer Nanocomposites, *J. Appl. Polym. Sci.*, 2022, **139**(14), e51904.
42 A. Haryńska, J. Kucinska-Lipka, A. Sulowska, I. Gubanska, M. Kostrzewa and H. Janik, Medical-Grade PCL Based Polyurethane System for FDM 3D Printing—Characterization and Fabrication, *Materials*, 2019, **12**, 887.
43 N. Vidakis, M. Petousis, N. K. Nasikas, T. Manios, N. Mountakis, J. Valsamos and E. Sfakiotakis, Optimization of the engineering response of medical-graded polycaprolactone (PCL) over multiple generic control parameters in bioplotting, *Int. J. Adv. Des. Manuf. Technol.*, 2024, **135**, 2373–2395.
44 N. Vidakis, M. Petousis, C. David, D. Sagris, N. Mountakis, S. Mariza, A. Moutsopoulou and N. K. Nasikas, Robust design optimization of Critical Quality Indicators (CQIs) of medical-graded polycaprolactone (PCL) in bioplotting, *Bioprinting*, 2024, e00361.
45 A. J. Arockiam, K. Subramanian, R. G. Padmanabhan, R. Selvaraj, D. K. Bagal and S. Rajesh, A review on PLA with different fillers used as a filament in 3D printing, *Mater. Today: Proc.*, 2022, **50**, 2057–2064.
46 N. Vidakis, D. Kalderis, N. Michailidis, V. Papadakis, N. Mountakis, A. Argyros, M. Spiridaki, A. Moutsopoulou and M. Petousis, Environmentally friendly Polylactic Acid/Ferronickel slag composite filaments for material extrusion 3D printing: A comprehensive optimization of the filler content, *Mater. Today Sustain.*, 2024, 100881.
47 N. Vidakis, M. Petousis, N. Michailidis, V. Papadakis, N. Mountakis, A. Argyros, E. Dimitriou, C. Charou and A. Moutsopoulou, Polylactic acid/silicon nitride biodegradable and biomedical Nanocomposites with optimized rheological and thermomechanical response for material extrusion additive manufacturing, *Biomed. Eng. Adv.*, 2023, **6**, 100103.
48 L. D'Arienzo, S. Acierno, A. Patti and L. Di Maio, Cellulose/Polyhydroxybutyrate (PHB) Composites as a Sustainable Bio-Based Feedstock to 3D-Printing Applications, *Materials*, 2024, **17**, 916.
49 M. Qahtani, F. Wu, M. Misra, S. Gregori, D. F. Mielewski and A. K. Mohanty, Experimental Design of Sustainable

3D-Printed Poly(Lactic Acid)/Biobased Poly(Butylene Succinate) Blends via Fused Deposition Modeling, *ACS Sustainable Chem. Eng.*, 2019, **7**, 14460–14470.
50 H. Torabi, H. McGreal, H. Zarrin and E. Behzadfar, Effects of Rheological Properties on 3D Printing of Poly(lactic acid) (PLA) and Poly(hydroxy alkenoate) (PHA) Hybrid Materials, *ACS Appl. Polym. Mater.*, 2023, **5**, 4034–4044.
51 Z. A. Raza, S. Abid and I. M. Banat, Polyhydroxyalkanoates: Characteristics, production, recent developments and applications, *Int. Biodeterior. Biodegrad.*, 2018, **126**, 45–56.
52 K. Khatami, M. Perez-Zabaleta, I. Owusu-Agyeman and Z. Cetecioglu, Waste to bioplastics: How close are we to sustainable polyhydroxyalkanoates production?, *Waste Manage.*, 2021, **119**, 374–388.
53 A. Naseem, I. Rasul, Z. Ali Raza, F. Muneer, A. ur Rehman and H. Nadeem, Bacterial production of polyhydroxyalkanoates (PHAs) using various waste carbon sources, *PeerJ*, 2024, **12**, e17936.
54 C. M. Chan, S. Pratt, P. Halley, D. Richardson, A. Werker, B. Laycock and L.-J. Vandi, Mechanical and physical stability of polyhydroxyalkanoate (PHA)-based wood plastic composites (WPCs) under natural weathering, *Polym. Test.*, 2019, **73**, 214–221.
55 M. Winnacker, Polyhydroxyalkanoates: Recent Advances in Their Synthesis and Applications, *Eur. J. Lipid Sci. Technol.*, 2019, **121**, 1900101.
56 G. Mannina, D. Presti, G. Montiel-Jarillo and M. E. Suárez-Ojeda, Bioplastic recovery from wastewater: A new protocol for polyhydroxyalkanoates (PHA) extraction from mixed microbial cultures, *Bioresour. Technol.*, 2019, **282**, 361–369.
57 P. C. Sabapathy, S. Devaraj, K. Meixner, P. Anburajan, P. Kathirvel, Y. Ravikumar, H. M. Zabed and X. Qi, Recent developments in Polyhydroxyalkanoates (PHAs) production – A review, *Bioresour. Technol.*, 2020, **306**, 123132.
58 B. Cecen, FDM-based 3D printing of PLA/PHA composite polymers, *Chem. Pap.*, 2023, **77**, 4379–4386.
59 G. Torğut and N. Gürler, Nanofiller reinforced biodegradable PHA/PLA composites: physico-chemical, thermal and dielectric properties, *J. Polym. Res.*, 2021, **28**, 452.
60 A. Thakur, M. Musiol, K. Duale and M. Kowalczuk, Navigating the Future of PHA Composites: A Review of Challenges and Opportunities, 2024, DOI: **10.20944/preprints202405.1308.v1**.
61 H. Torabi, H. McGreal, H. Zarrin and E. Behzadfar, Effects of Rheological Properties on 3D Printing of Poly(lactic acid) (PLA) and Poly(hydroxy alkenoate) (PHA) Hybrid Materials, *ACS Appl. Polym. Mater.*, 2023, **5**, 4034–4044.
62 Data Bridge Market Research, Global Polyhydroxyalkanoates (PHA) Market – Industry Trends and Forecast to 2031, 2024.
63 Statista, Market value of polyhydroxyalkanoate (PHA) worldwide in 2022, with a forecast for 2029, 2024.
64 Global Market Insights, Polyhydroxyalkanoate (PHA) Market – By Product, PHA Type, Production Methods, Application Analysis, Share, Growth Forecast, 2025–2034, 2024.
65 K. Qian, A. Kumar, H. Zhang, D. Bellmer and R. Huhnke, Recent advances in utilization of biochar, *Renewable Sustainable Energy Rev.*, 2015, **42**, 1055–1064.
66 K. Thepsuthammarat, A. Reungsang and P. Plangklang, Microalga Coelastrella sp. Cultivation on Unhydrolyzed Molasses-Based Medium towards the Optimization of Conditions for Growth and Biomass Production under Mixotrophic Cultivation, *Molecules*, 2023, **28**, 3603.
67 J. Cui, J. Liu, X. Chen, J. Meng, S. Wei, T. Wu, Y. Wang, Y. Xie, C. Lu and X. Zhang, Ganoderma Lucidum-derived erythrocyte-like sustainable materials, *Carbon*, 2022, **196**, 70–77.
68 C. Xu, M. Nasrollahzadeh, M. Sajjadi, M. Maham, R. Luque and A. R. Puente-Santiago, Benign-by-design nature-inspired nanosystems in biofuels production and catalytic applications, *Renewable Sustainable Energy Rev.*, 2019, **112**, 195–252.
69 R. Mandala, B. A. Prasad and S. Akella, Development and characterization of groundnut shell-derived biocarbon-reinforced polylactic acid composite filaments for FDM, *J. Appl. Polym. Sci.*, 2024, **141**, e55689.
70 R. D. Maalihan, L. I. B. Briones, E. P. Canarias and G. P. Lanuza, On the 3D printing and flame retardancy of expandable graphite-coated polylactic acid, *Mater. Today: Proc.*, 2023, DOI: **10.1016/j.matpr.2023.09.140**.
71 S. K. Mohanty, R. Valenca, A. W. Berger, I. K. M. Yu, X. Xiong, T. M. Saunders and D. C. W. Tsang, Plenty of room for carbon on the ground: Potential applications of biochar for stormwater treatment, *Sci. Total Environ.*, 2018, **625**, 1644–1658.
72 S. Sahota, V. K. Vijay, P. M. V. Subbarao, R. Chandra, P. Ghosh, G. Shah, R. Kapoor, V. Vijay, V. Koutu and I. S. Thakur, Characterization of leaf waste based biochar for cost effective hydrogen sulphide removal from biogas, *Bioresour. Technol.*, 2018, **250**, 635–641.
73 C. Zhang, L. Liu, M. Zhao, H. Rong and Y. Xu, The environmental characteristics and applications of biochar, *Environ. Sci. Pollut. Res.*, 2018, **25**, 21525–21534.
74 J. Wang and S. Wang, Preparation, modification and environmental application of biochar: A review, *J. Cleaner Prod.*, 2019, **227**, 1002–1022.
75 S. Wijitkosum, Biochar derived from agricultural wastes and wood residues for sustainable agricultural and environmental applications, *Int. Soil Water Conserv. Res.*, 2022, **10**, 335–341.
76 D. Rathnayake, H. Schmidt, J. Leifeld, J. Mayer, C. A. Epper, T. D. Bucheli and N. Hagemann, Biochar from animal manure: A critical assessment on technical feasibility, economic viability, and ecological impact, *GCB Bioenergy*, 2023, **15**, 1078–1104.
77 L. Zhao, Z.-F. Sun, X.-W. Pan, J.-Y. Tan, S.-S. Yang, J.-T. Wu, C. Chen, Y. Yuan and N.-Q. Ren, Sewage sludge derived biochar for environmental improvement: Advances, challenges, and solutions, *Water Res.: X*, 2023, **18**, 100167.
78 X. Chen, H.-Z. He, G.-K. Chen and H.-S. Li, Effects of biochar and crop straws on the bioavailability of cadmium in contaminated soil, *Sci. Rep.*, 2020, **10**, 9528.
79 J. Liu, S. Huang, K. Chen, T. Wang, M. Mei and J. Li, Preparation of biochar from food waste digestate: Pyrolysis

behavior and product properties, *Bioresour. Technol.*, 2020, **302**, 122841.
80 S. Joseph, A. L. Cowie, L. Van Zwieten, N. Bolan, A. Budai, W. Buss, M. L. Cayuela, E. R. Graber, J. A. Ippolito, Y. Kuzyakov, Y. Luo, Y. S. Ok, K. N. Palansooriya, J. Shepherd, S. Stephens, Z. (Han) Weng and J. Lehmann, How biochar works, and when it doesn't: A review of mechanisms controlling soil and plant responses to biochar, *GCB Bioenergy*, 2021, **13**, 1731–1764.
81 S. Varjani, G. Kumar and E. R. Rene, Developments in biochar application for pesticide remediation: Current knowledge and future research directions, *J. Environ. Manage.*, 2019, **232**, 505–513.
82 T. Almeelbi, Magnetite Biochar Derived from Date Palm Tree Waste Leaves for Adsorption of Congo Red from Aqueous Solution, *Egypt. J. Chem.*, 2025, **68**, 205–212.
83 H. Al-Khalaifah and A. Al-Nasser, Critical review on the use of biochar in poultry industry: benefits, characteristics and applications, *Worlds Poult. Sci. J.*, 2023, **79**, 807–833.
84 S. Fan, L. Cui, H. Li, M. Guang, H. Liu, T. Qiu and Y. Zhang, Value-added biochar production from microwave pyrolysis of peanut shell, *Int. J. Chem. React. Eng.*, 2023, **21**, 1035–1046.
85 P. R. Yaashikaa, P. S. Kumar, S. Varjani and A. Saravanan, A critical review on the biochar production techniques, characterization, stability and applications for circular bioeconomy, *Biotechnol. Rep.*, 2020, **28**, e00570.
86 Z. Shen, D. Hou, B. Zhao, W. Xu, Y. S. Ok, N. S. Bolan and D. S. Alessi, Stability of heavy metals in soil washing residue with and without biochar addition under accelerated ageing, *Sci. Total Environ.*, 2018, **619–620**, 185–193.
87 D. O'Connor, T. Peng, G. Li, S. Wang, L. Duan, J. Mulder, G. Cornelissen, Z. Cheng, S. Yang and D. Hou, Sulfur-modified rice husk biochar: A green method for the remediation of mercury contaminated soil, *Sci. Total Environ.*, 2018, **621**, 819–826.
88 J. Beiyuan, Y. M. Awad, F. Beckers, J. Wang, D. C. W. Tsang, Y. S. Ok, S.-L. Wang, H. Wang and J. Rinklebe, (Im)mobilization and speciation of lead under dynamic redox conditions in a contaminated soil amended with pine sawdust biochar, *Environ. Int.*, 2020, **135**, 105376.
89 Y. Wu, Y. Xia, X. Jing, P. Cai, A. D. Igalavithana, C. Tang, D. C. W. Tsang and Y. S. Ok, Recent advances in mitigating membrane biofouling using carbon-based materials, *J. Hazard. Mater.*, 2020, **382**, 120976.
90 P. Zhang, D. O'Connor, Y. Wang, L. Jiang, T. Xia, L. Wang and D. C. W. Tsang, Y. S. Ok and D. Hou, A green biochar/iron oxide composite for methylene blue removal, *J. Hazard. Mater.*, 2020, **384**, 121286.
91 K. N. Palansooriya, Y. Yang, Y. F. Tsang, B. Sarkar, D. Hou, X. Cao, E. Meers, J. Rinklebe, K.-H. Kim and Y. S. Ok, Occurrence of contaminants in drinking water sources and the potential of biochar for water quality improvement: A review, *Crit. Rev. Environ. Sci. Technol.*, 2020, **50**, 549–611.
92 J. Liu, B. Jiang, J. Shen, X. Zhu, W. Yi, Y. Li and J. Wu, Contrasting effects of straw and straw-derived biochar applications on soil carbon accumulation and nitrogen use efficiency in double-rice cropping systems, *Agric., Ecosyst. Environ.*, 2021, **311**, 107286.
93 F. Yang, C. Wang and H. Sun, A comprehensive review of biochar-derived dissolved matters in biochar application: Production, characteristics, and potential environmental effects and mechanisms, *J. Environ. Chem. Eng.*, 2021, **9**, 105258.
94 N. Cheng, B. Wang, P. Wu, X. Lee, Y. Xing, M. Chen and B. Gao, Adsorption of emerging contaminants from water and wastewater by modified biochar: A review, *Environ. Pollut.*, 2021, **273**, 116448.
95 L. Wang, D. Hou, Y. Cao, Y. S. Ok, F. M. G. Tack, J. Rinklebe and D. O'Connor, Remediation of mercury contaminated soil, water, and air: A review of emerging materials and innovative technologies, *Environ. Int.*, 2020, **134**, 105281.
96 L. Ye, Z. Peng, L. Wang, A. Anzulevich, I. Bychkov, D. Kalganov, H. Tang, M. Rao, G. Li and T. Jiang, Use of Biochar for Sustainable Ferrous Metallurgy, *JOM*, 2019, **71**, 3931–3940.
97 S. K. Das, G. K. Ghosh and R. Avasthe, Application of biochar in agriculture and environment, and its safety issues, *Biomass Convers Biorefin*, 2023, **13**, 1359–1369.
98 M. Legan, A. Ž. Gotvajn and K. Zupan, Potential of biochar use in building materials, *J. Environ. Manage.*, 2022, **309**, 114704.
99 K. Weber and P. Quicker, Properties of biochar, *Fuel*, 2018, **217**, 240–261.
100 R. V. Hemavathy, P. S. Kumar, K. Kanmani and N. Jahnavi, Adsorptive separation of Cu(II) ions from aqueous medium using thermally/chemically treated Cassia fistula based biochar, *J. Cleaner Prod.*, 2020, **249**, 119390.
101 R. Gayathri, K. P. Gopinath and P. S. Kumar, Adsorptive separation of toxic metals from aquatic environment using agro waste biochar: Application in electroplating industrial wastewater, *Chemosphere*, 2021, **262**, 128031.
102 Fortune Buisiness Insights, Biochar Market Size, Share & Industry Analysis, By Technology (Pyrolysis and Gasification), By Application (Farming, Livestock, Power Generation, and Others), and Regional Forecast, 2024–2032 Source: **https://www.fortunebusinessinsights.com/industry-reports/biochar-market-100750**, 2024.
103 Maximize Market Research, Biochar Market: Global Industry Analysis and Forecast (2024–2030), 2024.
104 P. Anerao, A. Kulkarni, Y. Munde, A. Shinde and O. Das, Biochar reinforced PLA composite for fused deposition modelling (FDM): A parametric study on mechanical performance, *Compos., Part C: Open Access*, 2023, **12**, 100406.
105 Z. Mohammed, S. Jeelani and V. Rangari, Effective reinforcement of engineered sustainable biochar carbon for 3D printed polypropylene biocomposites, *Compos., Part C: Open Access*, 2022, **7**, 100221.
106 M. Idrees, S. Jeelani and V. Rangari, Three-Dimensional-Printed Sustainable Biochar-Recycled PET Composites, *ACS Sustainable Chem. Eng.*, 2018, **6**, 13940–13948.
107 N. Vidakis, D. Kalderis, M. Petousis, E. Maravelakis, N. Mountakis, N. Bolanakis and V. Papadakis, Biochar

filler in MEX and VPP additive manufacturing: characterization and reinforcement effects in polylactic acid and standard grade resin matrices, *Biochar*, 2023, **5**, 39.

108 M. Petousis, E. Maravelakis, D. Kalderis, V. Saltas, N. Mountakis, M. Spiridaki, N. Bolanakis, A. Argyros, V. Papadakis, N. Michailidis and N. Vidakis, Biochar for sustainable additive manufacturing: Thermal, mechanical, electrical, and rheological responses of polypropylene-biochar composites, *Biomass Bioenergy*, 2024, **186**, 107272.

109 N. Vidakis, M. Petousis, D. Kalderis, N. Michailidis, E. Maravelakis, V. Saltas, N. Bolanakis, V. Papadakis, A. Argyros, N. Mountakis and M. Spiridaki, A coherent engineering assessment of ABS/biochar biocomposites in MEX 3D additive manufacturing, *Heliyon*, 2024, **10**, e32094.

110 N. Vidakis, M. Petousis, D. Kalderis, N. Michailidis, E. Maravelakis, V. Saltas, N. Bolanakis, V. Papadakis, M. Spiridaki and A. Argyros, Reinforced HDPE with optimized biochar content for material extrusion additive manufacturing: morphological, rheological, electrical, and thermomechanical insights, *Biochar*, 2024, **6**, 37.

111 N. Vidakis, M. Petousis, D. Sagris, C. David, N. Mountakis, M. Spiridaki, E. Maravelakis, C. Charitidis and E. Stratakis, Enhancing biocomposite critical quality indicators (CQIs): the impact of biochar content in additive manufacturing, *Biochar*, 2025, **7**, 22.

112 N. Bolanakis, N. Vidakis, M. Petousis, D. Kalderis, D. Galanakis, N. Mountakis and E. Maravelakis, in 2024 5th International Conference in Electronic Engineering, Information Technology & Education (EEITE), 2024, pp. 1–8.

113 T. Tsubota, S. Tsuchiya, T. Kusumoto and D. Kalderis, Assessment of Biochar Produced by Flame-Curtain Pyrolysis as a Precursor for the Development of an Efficient Electric Double-Layer Capacitor, *Energies*, 2021, **14**, 7671.

114 Y. Song and Q. Zheng, Concepts and conflicts in nanoparticles reinforcement to polymers beyond hydrodynamics, *Prog. Mater. Sci.*, 2016, **84**, 1–58.

115 Y. Zare, K. Y. Rhee and D. Hui, Influences of nanoparticles aggregation/agglomeration on the interfacial/interphase and tensile properties of nanocomposites, *Composites, Part B*, 2017, **122**, 41–46.

116 Y. A. Badr, K. M. Abd El-Kader and R. M. Khafagy, Raman spectroscopic study of CdS, PVA composite films, *J. Appl. Polym. Sci.*, 2004, **92**, 1984–1992.

117 A. V. Veluthandath and P. B. Bisht, Identification of Whispering Gallery Mode (WGM) coupled photoluminescence and Raman modes in complex spectra of MoS_2 in Polymethyl methacrylate (PMMA) microspheres, *J. Lumin.*, 2017, **187**, 255–259.

118 V. Resta, G. Quarta, M. Lomascolo, L. Maruccio and L. Calcagnile, Raman and Photoluminescence spectroscopy of polycarbonate matrices irradiated with different energy 28Si+ ions, *Vacuum*, 2015, **116**, 82–89.

119 B. H. Stuart, Temperature studies of polycarbonate using Fourier transform Raman spectroscopy, *Polym. Bull.*, 1996, **36**, 341–346.

120 M. D. Peris-Díaz, B. Łydżba-Kopczyńska and E. Sentandreu, Raman spectroscopy coupled to chemometrics to discriminate provenance and geological age of amber, *J. Raman Spectrosc.*, 2018, **49**, 842–851.

121 M. Makarem, C. M. Lee, K. Kafle, S. Huang, I. Chae, H. Yang, J. D. Kubicki and S. H. Kim, Probing cellulose structures with vibrational spectroscopy, *Cellulose*, 2019, **26**, 35–79.

122 C. Zimmerer, I. Matulaitiene, G. Niaura, U. Reuter, A. Janke, R. Boldt, V. Sablinskas and G. Steiner, Nondestructive characterization of the polycarbonate–octadecylamine interface by surface enhanced Raman spectroscopy, *Polym. Test.*, 2019, **73**, 152–158.

123 D. V. de Sousa, L. M. Guimarães, J. F. Félix, J. C. Ker, C. E. R. G. Schaefer and M. J. Rodet, Dynamic of the structural alteration of biochar in ancient Anthrosol over a long timescale by Raman spectroscopy, *PLoS One*, 2020, **15**, e0229447.

124 C. Hu, X. Chen, J. Chen, W. Zhang and M. Q. Zhang, Observation of mutual diffusion of macromolecules in PS/PMMA binary films by confocal Raman microscopy, *Soft Matter*, 2012, **8**, 4780–4787.

125 L. Sandanamsamy, J. Mogan, N. A. Halim, W. S. W. Harun, K. Kadirgama and D. Ramasamy, A review on 3D printing bio-based polymer composite, *IOP Conf. Ser.: Mater. Sci. Eng.*, 2021, **1078**, 012031.

126 A. Giubilini, M. Messori, F. Bondioli, P. Minetola, L. Iuliano, G. Nyström, K. Maniura-Weber, M. Rottmar and G. Siqueira, 3D-Printed Poly(3-hydroxybutyrate-*co*-3-hydroxyhexanoate)-Cellulose-Based Scaffolds for Biomedical Applications, *Biomacromolecules*, 2023, **24**, 3961–3971.